JOURNAL OF MATERIALS SCIENCE 17 (1982) 2112–2126

The effect of sulphide inclusions on fracture toughness and fatigue crack growth in 12 wt% Cr steels

V. P. RAGHUPATHY, V. SRINIVASAN*, H. KRISHNAN, M. N. CHANDRASEKHARAIAH
Corporate Research & Development Division, Bharat Heavy Electricals Limited, Hyderabad 500593, India

The variation of plane strain fracture toughness and fatigue crack growth rates with sulphide inclusion content has been examined for four different sulphur levels in a 12 wt% Cr stainless steel. Charpy impact tests have also been conducted and the experimental results are correlated with the volume fraction of inclusions and the inter-inclusion spacing. The availability of the experimental results for the case of steam turbine blading is discussed with a hypothetical example problem.

1. Introduction

The effects of microstructure and impurities on the fracture toughness and fatigue crack growth of steels is generally well recognized. Among the different types of inclusions present in steels, sulphide inclusions have by far the most deleterious effect due to their deformability under hot working conditions.

Three distinct morphologies of sulphide inclusions have been identified by Sims [1]. The deleterious effects of sulphide inclusions on plane strain fracture toughness of some medium and high strength steels have been demonstrated by Baker *et al.* [2]. Birkle *et al.* [3] showed that the crack growth process in 0.45 C–Ni–Cr–Mo steels occurs by the nucleation of voids at sulphide inclusions and their subsequent coalescence. Thus, the fracture toughness and fatigue crack growth rates are essentially determined by the size and distribution of sulphide inclusions, according to the empirical relationship due to Krafft [4] for the onset of plane strain fracture instability. The Krafft relationship was subsequently modified [5] to take into account the triaxial state of stress at the crack tip under plane strain conditions. Thus, microvoid nucleation and coalescence mode of fracture seems to be a necessary condition to determine the detrimental effects of higher sulphur content or the advantageous effects of reduced sulphur content obtained by the electroslag refining process. Experiments done under these conditions on $2\frac{1}{4}$ Cr–1 Mo steels demonstrated that the sulphur content has a large deleterious effect near or above nil ductility transition temperature (NDTT) where microvoid coalescence occurs, but it has no significant effect at lower temperatures where cleavage occurs [6]. Consequently, lower shelf energy and fracture appearance transition temperature (FATT) alone do not completely describe the harmful effects of inclusions on fracture in a meaningful manner [7].

The mechanical anisotropy caused by the elongated shape of inclusions in hot rolled steels is reflected again in ductility, impact energy or upper shelf energy and crack opening displacement (COD) or fracture toughness. Information on the effect of inclusions on these properties is sporadic for the case of medium strength steels and particularly so for 12% Cr steels [8, 9]. The present investigation was undertaken to establish fracture toughness and fatigue crack growth data for 12% Cr steels as a function of sulphur content and to study their relationship with the volume fraction of sulphide inclusions and inter-inclusion spacing.

*Present address: National Aeronautical Laboratory, Bangalore, India.

0022–2461/82/072112–15$04.30/0

TABLE I Chemical composition of desulphurized, as-received and resulphurized steels

Batch code	Contents (wt %)					
	C	S	Cr	Mn	Si	Ni
S–30	0.20	0.003 to 0.005	13.0	0.49	0.35	0.46
S–110	0.18	0.011 to 0.013	13.3	0.55	0.37	0.39
S–200	0.21	0.020 to 0.023	12.4	0.45	0.41	0.38
S–340	0.20	0.034 to 0.036	12.6	0.42	0.46	0.51

2. Experimental procedure

2.1. Materials

The material used in the present investigation is commonly used for low pressure blading applications in steam turbines. The as received material, in the form of bars, had a nominal composition indicated in Table I with a sulphur content of 110 ppm. The material, in batches of 15 kg, was remelted in an induction furnace. Resulphurization was done by adding known amounts of pyrites (FeS) to the molten metals to obtain sulphur levels of 220 ppm and 340 ppm. Major alloying elements in the form of ferro alloys were added to compensate for the losses due to melting. Desulphurization to a sulphur level of 30 ppm was achieved by electroslag refining of the supplied steel.

Ingots with sulphur levels of 30 ppm, 110 ppm, 200 ppm and 340 ppm, thus obtained, were homogenized at 1000° C for 60 h. They were then hot forged in the temperature range 1000 to 1050° C. Chemical compositions of these steels are given in Table I.

The forged bars were machined to obtain tensile, Charpy impact, compact tension and fatigue crack growth specimens and also small cubes for metallography. The specimens thus obtained were austenitized at 1020° C for 1 h, oil quenched and tempered at 670° C for 2 h.

The results of the tensile tests are given in Table II. Charpy impact tests were conducted on specimens of all sulphur levels at different temperatures from − 190 to + 200° C. The calculated upper shelf energy values are also given in Table II.

2.2. Fracture toughness testing

Fracture toughness tests were conducted on compact tension specimens of thickness 12.7 mm (0.5 in) and 18.25 mm (0.75 in) with a chevron notch in accordance with ASTM E 399 standards. The samples were pre-cracked in a subresonant fatigue machine and the crack opening was followed using a clip gauge. The results are listed in Table III.

2.3. Fatigue crack growth testing

Fatigue crack propagation tests on centre notched flat specimens were conducted at room temperature. The specimens were 50 mm wide, 1.5 mm thick with a 4.5 mm x 0.5 mm centre notch produced by spark erosion. The frequency of loading was about 25 Hz. The crack extension was measured as a function of number of cycles using a stroboscope and a travelling microscope. The applied maximum stress was varied from 140 to 350 MPa. Stress ratios of 0.1, 0.3 and 0.5 were chosen and eight specimens were tested at each stress ratio corresponding to each sulphur level.

From the plots of half crack length, a, and the number of cycles, N, the crack growth rates da/dN and the corresponding stress intensity range ΔK, were calculated. The da/dN values were plotted against ΔK values for all the cases to obtain the crack growth rate curves indicating the three stages as reported in the literature. Least square analyses were carried out to fit the data points in stage II of the curve to evaluate the constant A and the exponent m, of the Paris–Erdogan relationship [10].

$$da/dN = A(\Delta K)^m, \quad (1)$$

TABLE II Mechanical properties

Batch code	0.2% proof stress (MPa)	Ultimate tensile strength (MPa)	Elongation (%)	Reduction in area (%)	Strain hardening coefficient	Upper shelf energy E_{us} (NM)
S–30	696.00	814.00	17.2	61.27	0.048	155.00
S–110	664.37	807.39	19.7	66.57	0.064	137.70
S–200	637.95	789.60	17.9	64.92	0.054	87.27
S–340	658.34	785.65	15.6	64.24	0.052	82.32

TABLE III Results of the fracture toughness tests

Batch code	Thickness of the test specimen (mm)	Near valid K_{Ic} (MPa $m^{1/2}$)	Average K_{Ic} (MPa $m^{1/2}$)	B_{min} (mm)	B'_{min} (mm)
S–30	11.80	91.67	91.70	43.58	23.37
	12.72	87.49		39.59	21.28
	12.84	91.89		43.50	23.48
	18.20	95.74		47.30	25.48
S–110	12.82	86.27	80.23	42.14	21.69
	12.83	79.62		35.88	18.48
	12.78	78.14		34.58	17.80
	18.20	78.04		34.52	17.75
	18.20	79.11		35.47	18.24
S–200	12.60	72.95	71.76	32.69	16.14
	12.60	67.39		27.90	13.78
	19.10	74.93		34.49	17.03
S–340	12.76	65.24	61.72	24.60	12.52
	12.68	63.16		23.61	11.74
	12.58	65.07		24.43	12.46
	17.70	53.43		16.42	8.40

$$\log (da/dN) = \log A + m \log (\Delta K), \quad (1a)$$

which is valid in stage II, where da/dN is the crack propagation rate in $msec^{-1}$ and ΔK the stress intensity range in MPa $\sqrt{m}$. The values of A and m are given in Table IV.

2.4. Metallographic examination

The heat treated cube-samples were examined in an optical microscope to determine their microstructure and also for quantitative evaluation of sulphide inclusions. All the four grades of steels showed a tempered martensitic structure (Fig. 1) with a prior austenite grain size of ASTM No. 7. For inclusion characterization, the polished surfaces of the samples were treated with aqueous silver nitrate. After this treatment, sulphides appear white under the optical microscope. About a hundred different fields were examined at a magnification of 1000X. Typical micrographs showing sulphide inclusions on surfaces bound by longitudinal and long transverse direction are shown in Fig. 2 and those bound by long transverse and short transverse directions are shown in Fig. 3.

TABLE IV Fatigue crack growth rate data

Batch code	Stress ratio, R	A (10^{-10})	m	ΔK_{Th} (MPa $m^{1/2}$)
S–30	0.1	1.08	2.04	13.0
	0.3	0.41	2.38	11.5
	0.5	1.61	1.97	7.4
S–110	0.1	0.40	2.40	13.0
	0.3	1.99	1.98	11.5
	0.5	1.61	2.01	7.4
S–200	0.1	0.61	2.24	13.5
	0.3	0.47	2.38	11.5
	0.5	0.53	2.40	7.9
S–340	0.1	0.33	2.43	14.0
	0.3	0.56	2.32	12.0
	0.5	0.80	2.23	8.0

Taking the linear dimensions of the inclusions as the characteristic length, histograms were prepared for steels of various sulphur levels. Figs 4 to 7 show histograms for sulphide inclusions both in the longitudinal and transverse directions.

The point counting method was adopted to find out the volume fraction, V_v, of sulphide inclusions. The area fraction A_A, which is equivalent to point fraction P_P, and volume fraction V_v, were also determined using a Quantimet 720. These values are given in Table V.

Using the intercept method, the number of feature intercepts (sulphides) per unit length N_L, was calculated. Number of sulphide inclusions per unit area N_A, was also calculated. These are listed in Table VI. The average size of sulphide inclusions $\bar{a}$, and the intersulphide inclusion spacing, λ, defined as the centre to centre distance, were calculated using the relationships [11]

$$\lambda = \left(\frac{\pi}{6V_v}\right)^{1/3} \bar{a}, \quad (2)$$

and

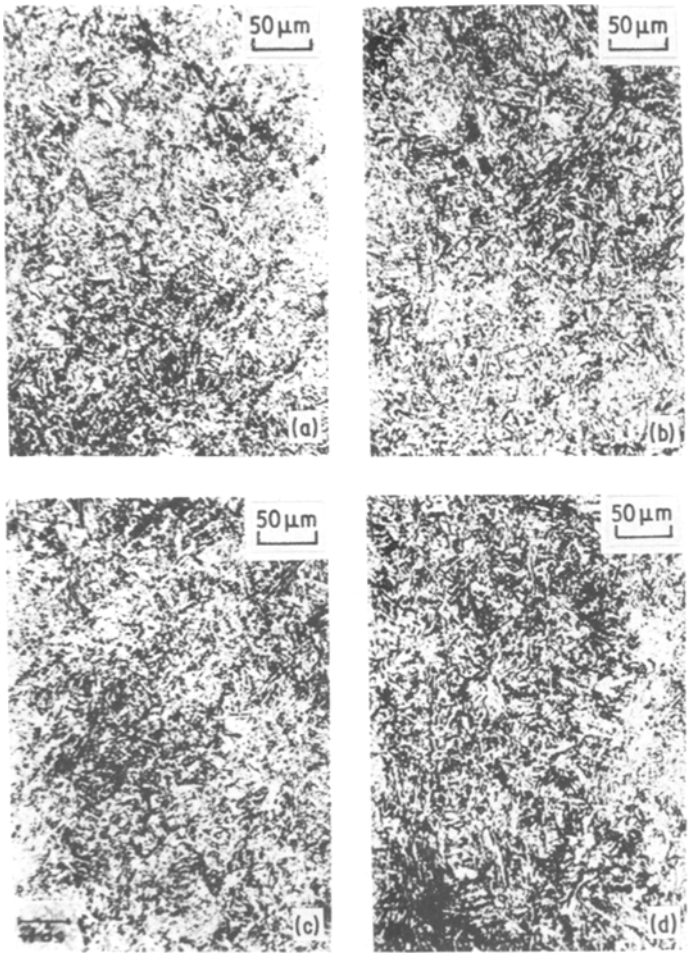

Figure 1 Microstructures of quenched and tempered 12% Cr steels (a) S–30 ppm, (b) S–110 ppm (c) S–200 ppm (d) S–340 ppm.

$$\bar{a} = \frac{V_v}{N_L}. \quad (3)$$

Table VI gives the values of $\bar{a}$ and λ for various steels.

3. Results and discussion

3.1. Fracture toughness, K_{Ic}

Fracture toughness tests were conducted on specimens of thickness 12.5 mm and 18.75 mm which were much smaller than the thickness recommended by ASTM E 399 (B_{min} in Table III). However, the critical stress intensity factor values are almost the same whether specimens of thickness 12.5 mm or 18.75 mm were tested. This observation implies that fracture is essentially under plane strain conditions in specimens of both thicknesses.

In steel S–340, only one specimen of thickness 18.75 mm could be tested. The critical stress intensity value is slightly lower than the values obtained from three specimens of thickness 12.5 mm (Table III). However, the ASTM E 399 thickness criterion was fulfilled in the 18.5 mm thick sample and hence the slightly lower value should be considered as due to experimental error or specimen to specimen scatter.

A number of other investigators [12, 13] have questioned the validity of the minimum thickness criteria set by the ASTM standards. Empirical thickness criteria determined for alloy steels [12] set the critical value as that giving about 85% square fracture in the broken test pieces, the remaining 15% comprising equal widths of slant fracture running along the side edges. The percentage shear lip was evaluated by actual measurement on the fracture surfaces and the values were either zero or less than 1% in all the cases. In addition, Ritter [13] has modified the ASTM minimum thickness (B_{min}) critierion to include the role of microstructure and the attainment of plane strain ahead of the crack tip to give a new

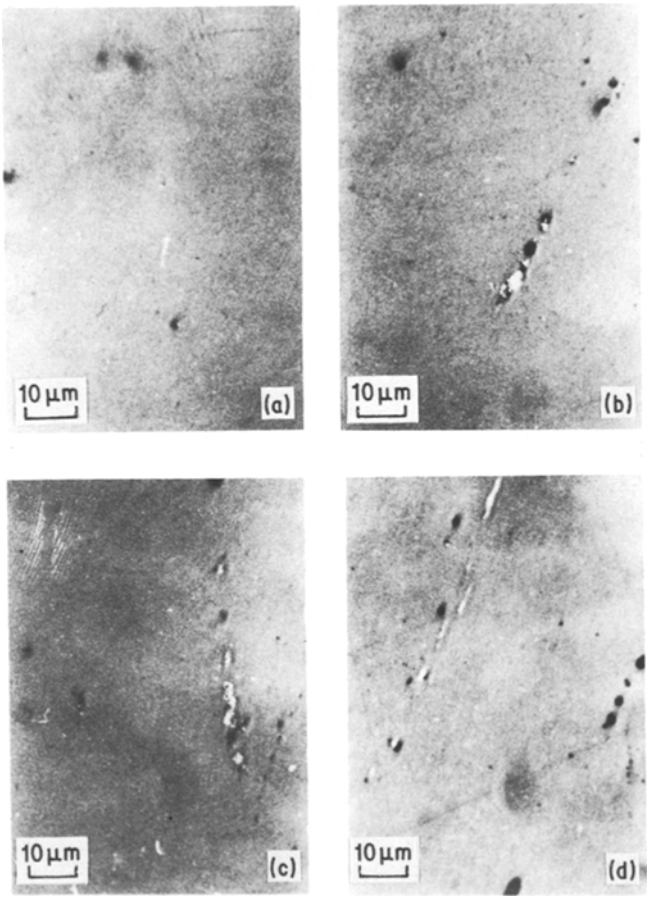

Figure 2 Optical micrographs showing sulphide inclusions (white) in the longitudinal section for 12% Cr steels (a) S–30 ppm (b) S–110 ppm (c) S–200 ppm (d) S–340 ppm.

minimum thickness, B'_{min}. His relationship

$$B'_{min} = 400 \frac{K_{Ic}^2}{E\sigma_{ys}}, \quad (4)$$

where σ_{ys} is the yield strength and E is Young's modulus suggests that comparatively thinner sections could be used to determine valid K_{Ic} values, particularly in medium and low strength steels. The B'_{min} value, calculated on the basis of the above expression, is also listed in Table III and it can be seen that the thicknesses used in the present investigation are well within these modified B_{min} values in a number of cases and that the K_{Ic} values are comparable in other cases. Thus it is concluded that the stress intensity values obtained in all the cases are the valid plane strain fracture toughness values, K_{Ic}.

3.2. Effect of sulphur level

The effect of the sulphur level on fracture toughness K_{Ic} is shown in Fig. 8 which also shows its dependance on volume fraction V_v of sulphides. Fracture toughness decreases nonlinearly as the sulphur concentration or the percentage volume fraction of sulphides is increased. Birkle *et al.* [3] have reported a similar relationship between K_{Ic} and sulphur level on a log–log plot.

A more meaningful correlation is obtained when fracture toughness K_{Ic} is plotted against the square root of the inter-sulphide inclusion spacing, λ. As λ increases (Fig. 9), K_{Ic} initially increases linearly up to $\lambda^{1/2} = 4.77 \times 10^{-3}\,m^{1/2}$. At higher values of $\lambda^{1/2}$ the plot tends to reach a plateau. This suggests that desulphurization to achieve sulphur concentrations less than 130 to 110 ppm does not significantly improve fracture toughness.

The inter-sulphide inclusion spacing may be approximated to the process zone size, d_T^3, so that the Krafft relationship [4]

$$K_{Ic} = En(2\pi d_T)^{1/2}, \quad (5)$$

where E is Young's modulus (206.8×10^3 MPa) and n is the strain hardening exponent (0.053) can

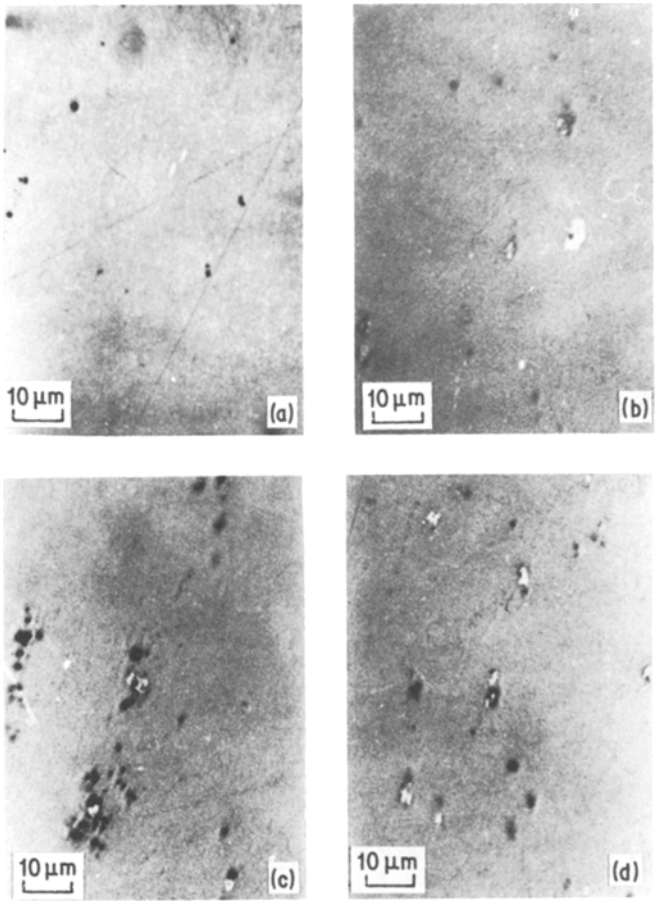

Figure 3 Optical micrographs showing sulphide inclusions (white) in the transverse direction for 12% Cr steels (a) S–30 ppm (b) S–110 ppm (c) S–200 ppm (d) S–340 ppm.

be used to evaluate the fracture toughness. K_{Ic} values, thus computed for all the four grades of steels, are listed in Table VII. The computed and the experimentally determined values show considerable variation. This variation is, perhaps, attributable to the fact that the Krafft model does not take into account the triaxial state of stress existing at the crack tip under plane strain conditions. This effect was subsequently included in the modified Krafft relation given by

$$K_{Ic} = E\left(\frac{\sigma_{ys} + \sigma_T}{E} + \frac{n}{2}\right)(2\pi d_T)^{1/2}, \quad (6)$$

where σ_{ys} is the yield (0.2% proof) strength in MPa and σ_T is the ultimate tensile strength in MPa.

Fracture toughness values, computed using Equation 6 show reasonable agreement (Table VII) with experimentally determined values of K_{Ic}.

Similar approaches to relate the stretched zone under plane strain conditions at the crack tip to the particle spacing have been attempted by other workers [11, 14] in the form

$$K_{Ic} = V_v^{-1/6}\left[2\left(\frac{\pi}{6}\right)^{1/3}\sigma_{ys}E\bar{a}\right]^{1/2}. \quad (7)$$

Using our experimental values of V_v and $\bar{a}$, the fracture toughness K_{Ic} has been evaluated and the results are given in Table VII. These values show better agreement with the experimental results.

In deriving Equation 7, Rice and Johnson [14] assumed that the heavily stretched region at the crack tip may be of the form

$$\delta \simeq 0.5\frac{K_{Ic}^2}{E\sigma_{ys}}, \quad (8)$$

and that δ may be of the order of inter-particle spacing λ. Experimental support for this assumption is provided in Table VIII, where the values of λ determined by the metallographic examination is correlated with the values of δ evaluated by taking the experimental values of K_{Ic} for different sulphur levels. Similar correlation between process zone size and inter-particle spacing has been reported by Birkle *et al.* [3]. However, they have

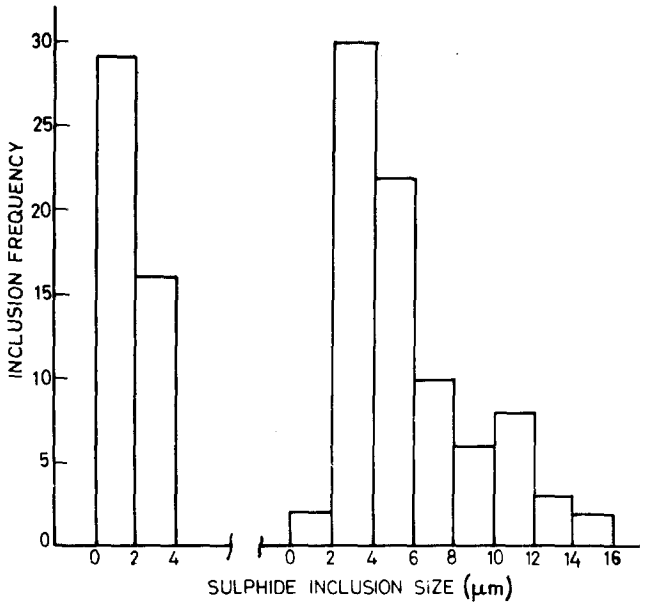

Figure 4 Histograms of sulphide inclusions for S–30 ppm steel.

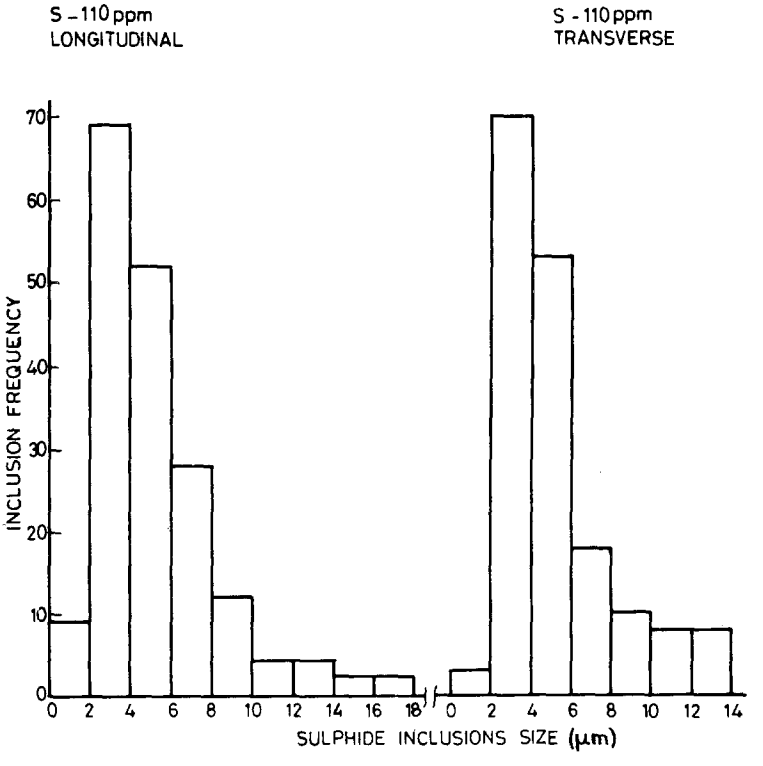

Figure 5 Histograms of sulphide inclusions for S–110 ppm steel.

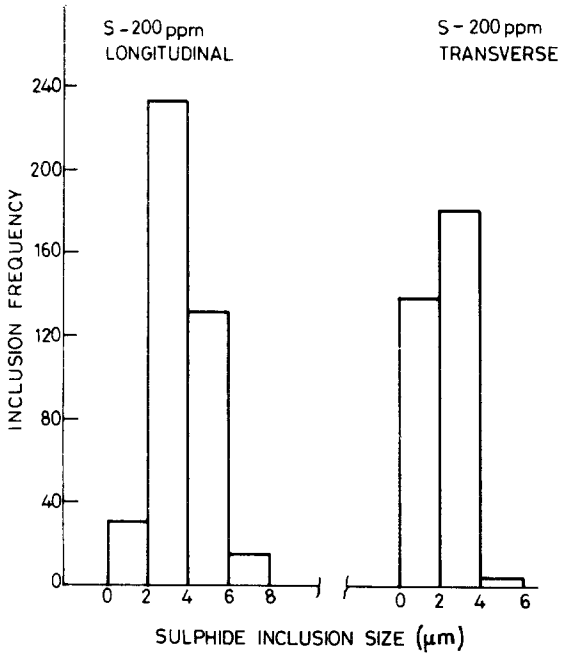

Figure 6 Histograms of sulphide inclusions for S–200 ppm steel.

computed the process zone size from the Krafft relationship (Equation 5) and obtained values of d_T in the range 2.50 to 6 μm. The present analysis based on Equation 8 is expected to be more accurate since the K_{Ic} values obtained from the Krafft relationship show considerable deviation from the experimentally obtained values. In addition, the average inclusion spacing has been computed using a relationship based on the surface area, while volumetric distribution of inclusion has been considered in the present case [11].

Sulphide inclusions of approximately 2 to 4 μm size occurred with maximum frequency in all the cases (Figs 4 to 7). It is, therefore, reasonable to expect their influence to be maximum. Thus, fracture toughness is expected to be effected by intermediate size particles rather than large or smaller ones. This provides experimental evidence to the doubts on particle size effects discussed by Broek [15]. Therefore, in calculating the inter-sulphide inclusion spacing, a constant value of inclusion size $\bar{a}$, which is the mean of four different values obtained in different steels (Table VI) is used.

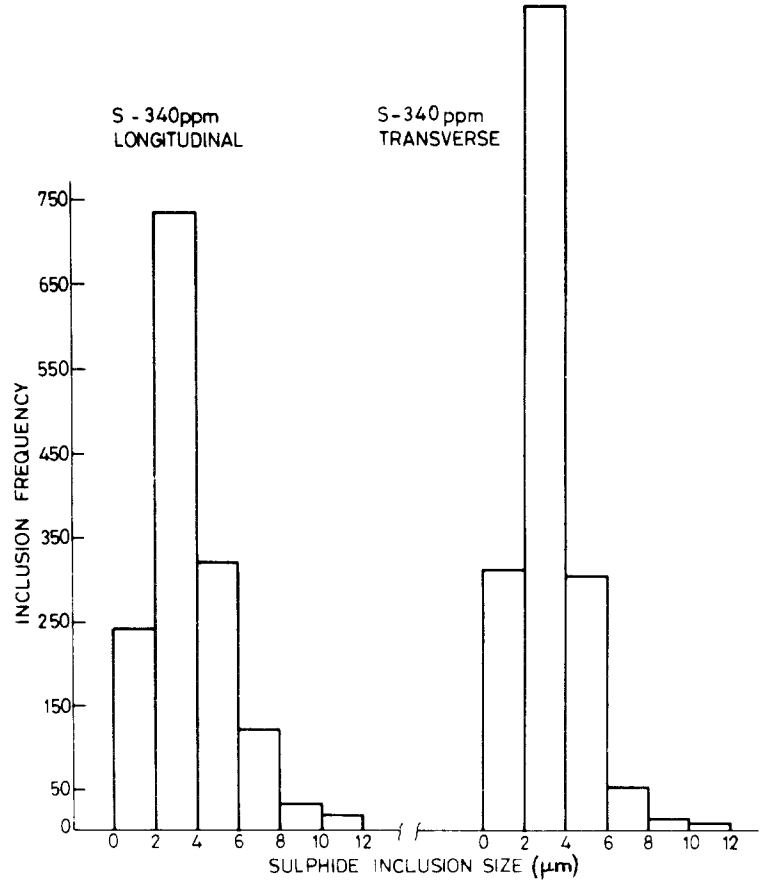

Figure 7 Histograms of sulphide inclusions for S–340 ppm steel.

TABLE V Quantitative metallographic data for sulphide inclusions

Batch code	A_A, Longitudinal (%)	A_A, Transverse (%)	P_P, Longitudinal (%)	P_P, Transverse (%)	V_v (%)
S–30	0.0145	0.0169	0.014	0.017	0.0156
S–110	0.0467	0.0824	0.056	0.069	0.0633
S–200	0.0970	0.1024	0.104	0.056	0.1011
S–340	0.1966	0.1955	0.175	–	0.1890

Further, the shape of the sulphide inclusions is often angular and is not elongated. Thus, there is no effect of aspect ratio (shape) on K_{Ic} that could be discerned in the present work.

The 1/6th power dependence of K_{Ic} on volume fraction V_v (Equation 7) was experimentally established by Hahn and Rosenfield [16]. The data from the present experiments are superposed on their values in Fig. 10 which shows a linear relationship between $K_{Ic}/(E\sigma_{ys})^{1/2}$ with V_v. The line is again parallel to the previous data but shifted upwards because of the lower values of σ_{ys}/E.

The Charpy impact strength, signified by the upper shelf energy, E_{us}, decreases with increase in sulphur content and shows similar behaviour to the fracture toughness, K_{Ic}, in that the value reaches a plateau around a value of 155 Nm (Fig. 9). The relationship between K_{Ic} and E_{us} is shown in Fig. 11 where $(K_{Ic}/\sigma_{ys})^2$ is plotted against E_{us}/σ_{ys}. A relationship of the type suggested by Rolfe [17]

$$\left(\frac{K_{Ic}}{\sigma_{ys}}\right)^2 = \frac{8.8 \times 10^{-2}}{\sigma_{ys}} (E_{us} - 2.72 \times 10^{-2} \sigma_{ys}) \quad (9)$$

is found to describe adequately the present results. The constants in Equation 9 are different from those in the empirical relationship of Rolfe. The reason for this difference might be that Charpy "V" notch energies at 26.5° C were used by Rolfe. The yield strength of the steels used in the present case are comparatively lower and also E_{us} has been used in view of its greater influence on the sulphur content.

TABLE VI Other quantitative metallographic parameters for sulphide inclusions

Batch code	N_A (mm^{-2})	N_L (mm^{-1})	$\bar{a}$ (μm)	λ (μm)
S–30	20.33	0.0659	2.363	36.34
S–110	69.15	0.1788	3.538	22.78
S–200	189.00	0.4732	2.136	19.48
S–340	638.40	1.1140	1.697	15.81

3.3. Fatigue crack growth rate

The value of m, the exponent in the Paris–Erdogan relationship (Equation 1) does not show any systematic variation either with stress ratio or with sulphur level. It varies between 1.49 and 2.43. Irwing and McCartney [18] have reported a value for m of 2.25 for martensitic steels. Nishioka *et al.* [19] have obtained a value of 2.3 for m and 4.1×10^{-9} for A for quenched and tempered 13% Cr steel of yield strength 60.4 kg mm^{-2} (592 MPa) tested with through thickness centre-notch specimens. The sulphur level was 150 ppm and the R value was 0.14. The corresponding values from Table IV are $m = 1.95$ and $A = 2.02 \times 10^{-10}$. The present experimental values are comparable and the small variations are attributable to experimental scatter.

It is possible to incorporate the effect of stress ratio, R, in the Paris–Erdogan relationship (Equation 1) by replacing the stress intensity range ΔK by the effective stress intensity range ΔK_{eff} where [20]

$$\Delta K_{eff} = \frac{1 - bR}{1 - R} \Delta K, \quad (10)$$

where $b = 0.85$ for $R > 0$. The modified Paris–Erdogan relationship is, therefore,

$$\frac{da}{dN} = A'(\Delta K_{eff})^{m'}. \quad (11)$$

To find ΔK_{eff}, the best fits obtained by least square analysis for each sulphur level at different stress ratios were used. Fig. 12 shows the correlation between the effective stress intensity range ΔK_{eff} and the crack propagation rate da/dN. The values of A' and m' obtained by least square analysis are 1.102×10^{-10} and 2.08 respectively.

In addition, data points in stage I were used to obtain estimates of threshold stress intensity range by extrapolation. These estimates, given in Table IV, show that ΔK_{Th} decreases with increasing stress ratio, R. A similar observation has been reported by Ohata and Sasaki [21].

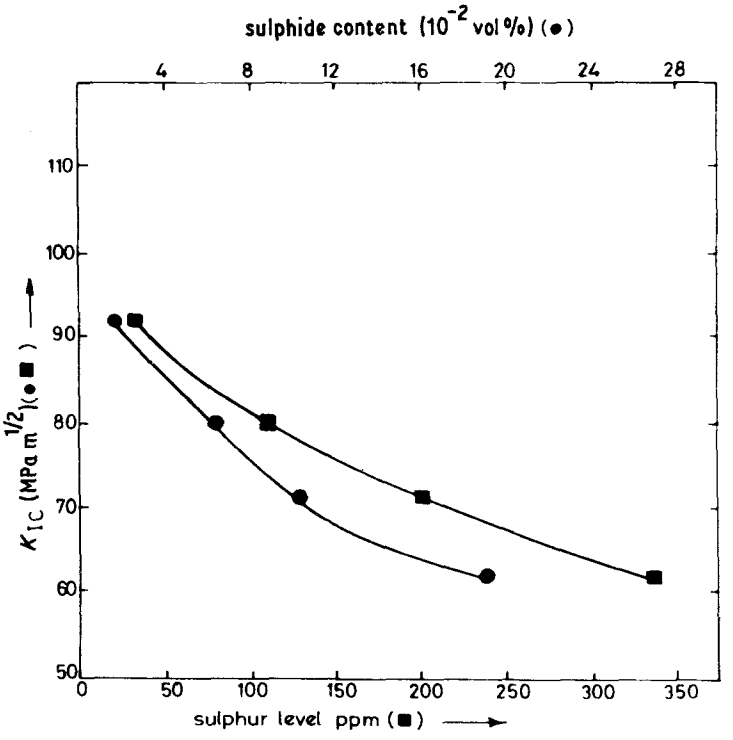

Figure 8 Plot showing the relationship between fracture toughness K_{Ic}, sulphur level and volume fraction V_v.

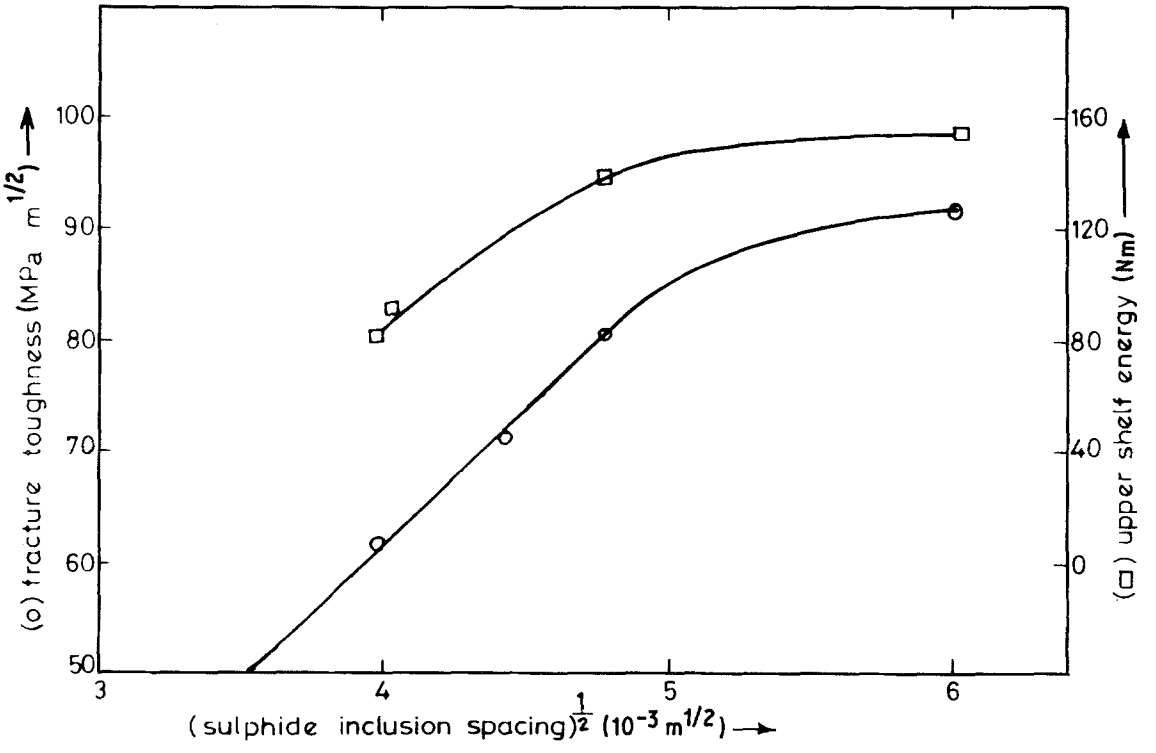

Figure 9 Relationship between fracture toughness K_{Ic}, upper shelf energy and inter-sulphide inclusion spacing.

TABLE VII Comparison of experimentally determined K_{Ic} with theoretically predicted models

Batch code	K_{Ic} Experimental (MPa $m^{1/2}$)	K_{Ic} Krafft model [4] (MPa $m^{1/2}$)	K_{Ic} Modified Krafft model [5] (MPa $m^{1/2}$)	K_{Ic} Rice-Johnson model [14] (MPa $m^{1/2}$)
S–30	91.70	165.63	101.00	104.73
S–110	80.23	131.13	79.51	79.16
S–200	71.56	121.27	73.03	70.31
S–340	61.72	109.25	65.99	61.45

3.4. Effect of sulphur level

Fig. 12 shows that the constants A' and m' do not depend either on the volume fraction of sulphide inclusions or on the number of (feature) intercepts. A careful analysis of the fatigue crack growth rate curves at different R values for each sulphur level revealed that the interval between the threshold stress intensity range ΔK_{Th} and critical stress intensity factor K_c, tends to increase with decrease in sulphur level. Also, both the threshold stress intensity range ΔK_{Th} and the stress level for unstable crack growth (end of stage III) increase with decrease in R value in all the cases. The variation of ΔK_{Th} as a function of sulphur level is, however, marginal in attributing a significant effect of sulphur content on the fatigue crack growth rates of different steels.

4. Application

The establishment of pertinent experimental data on fracture toughness and fatigue crack growth rate of 12 Cr steels at four different sulphur levels enables the evaluation of critical crack length and crack growth as a function of number of cycles of operation for application in the low pressure stages of a steam turbine.

Assuming the most deleterious defect to be a semielliptical surface flaw with a depth to length ($a/2c$) ratio of 0.2 which could occur at a tension load of 50% of the yield strength of the material, the critical flaw sizes for catastrophic failure was calculated for different sulphur levels using the expressions developed by Irwin [22, 23] and applied to steam turbine rotors by Greenberg *et al.* [24]. The results of critical flaw depth a_{Cr} and length $2c$, calculated from the expression

$$a_{Cr} = Q\left[\left(\frac{K_{Ic}}{\Delta\sigma}\right)^2 \times \frac{1}{1.21\pi}\right], \qquad Q = 1.405 \quad (12)$$

are presented in Table IX. As may be expected from the fracture toughness results, the crack tolerance in terms of a and $2c$ decreases with increase in sulphur content.

Assuming the same conditions, the cyclic life at normal operating conditions can also be evaluated. However, as discussed in Section 3.4, the effect of varying sulphur level of fatigue crack growth rate is too marginal to warrant the use of different A

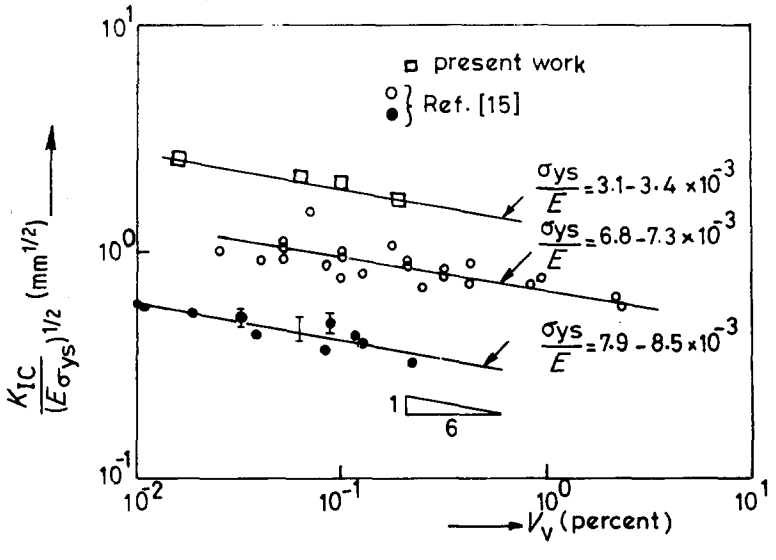

Figure 10 Relationship between volume fraction V_v and K_{Ic}.

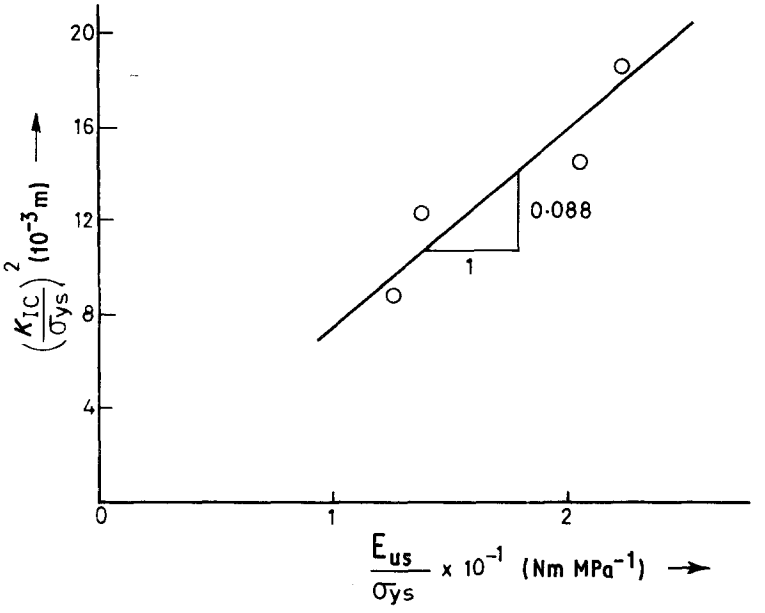

Figure 11 Relationship between fracture toughness $(K_{Ic}/\sigma_{ys})^2$ and E_{us}/σ_{ys}.

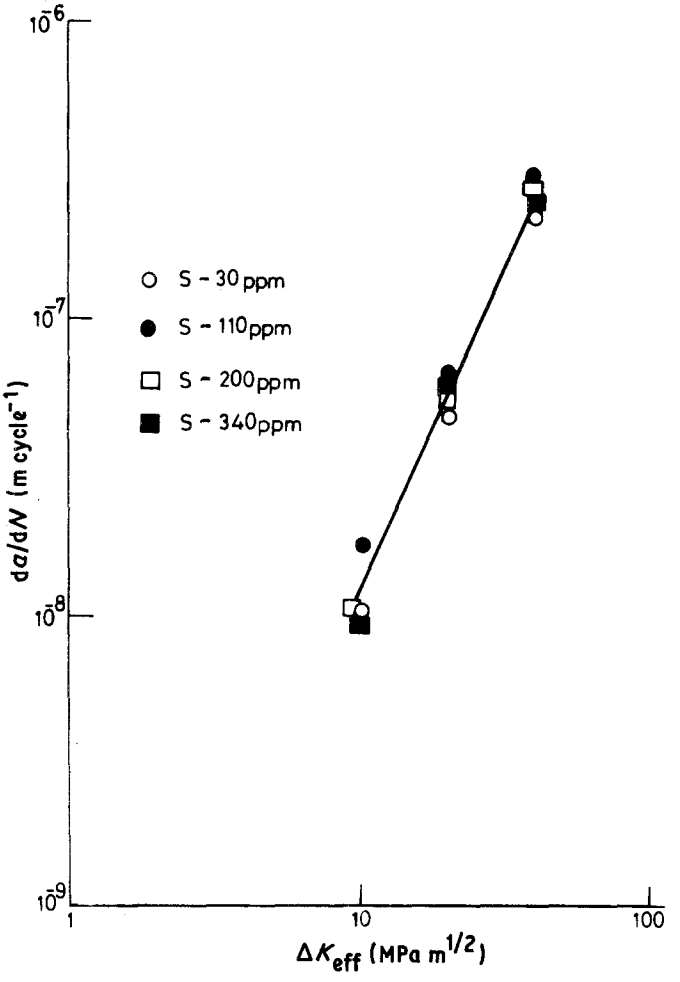

Figure 12 Relationship between fatigue crack growth rate and effective stress intensity range.

TABLE VIII Comparison of crack tip opening displacement with inter-sulphide spacing

Batch code	δ (μm)	λ (μm)
S–30	32.82	36.34
S–110	23.45	22.78
S–200	18.50	19.48
S–340	13.88	15.81

TABLE IX Critical depth and length for a semi-elliptical flaw

Batch code	$\Delta\sigma$ (MPa)	a_{Cr} (mm)	$2C = 5a$ (mm)
S–30	313.20	26.09	130.45
S–110	298.97	19.10	95.50
S–200	287.08	16.33	81.65
S–340	296.25	11.95	59.70

and m values given in Table IV. A regression analysis was, therefore, carried out for all the experimental data, for the case of $R = 0.1$, in the second stage of the fatigue crack growth curve. The results are presented in Fig. 13. The A and m values are 1.02×10^{-10} and 2.0966 respectively. Using these and the relevant applied stress and critical flaw size values, the number of elapsed cycles to failure can be calculated. Wessel *et al.* [25] have developed a generalized cyclic life expression which readily determines the number of cycles required for an existing defect to grow to the critical flaw size. The expression is given by

$$N = \frac{2}{(m-2)A\Delta\sigma^m M^{m/2}} \times \left[\frac{1}{a_i^{(m-2)/2}} - \frac{1}{a_{Cr}^{(m-2)/2}}\right] \quad \text{for } m \neq 2 \tag{13}$$

and

$$N = \frac{1}{AM\Delta\sigma^2} \ln \frac{a_{Cr}}{a_i} \qquad \text{for } m = 2$$

where M is the flaw shape and geometry parameter, which equals $1.21\pi/Q$ for surface defects, and a_i is the initial crack size.

Taking the experimental values of $\Delta\sigma$ for $R =$

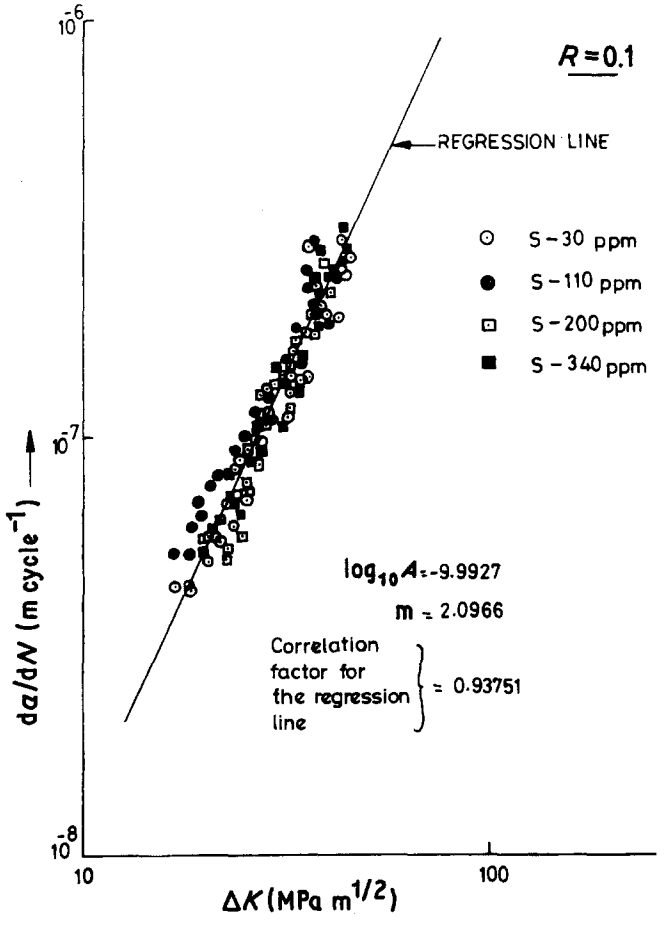

Figure 13 The second stage of fatigue crack growth rate curve of all the steels for $R = 0.1$.

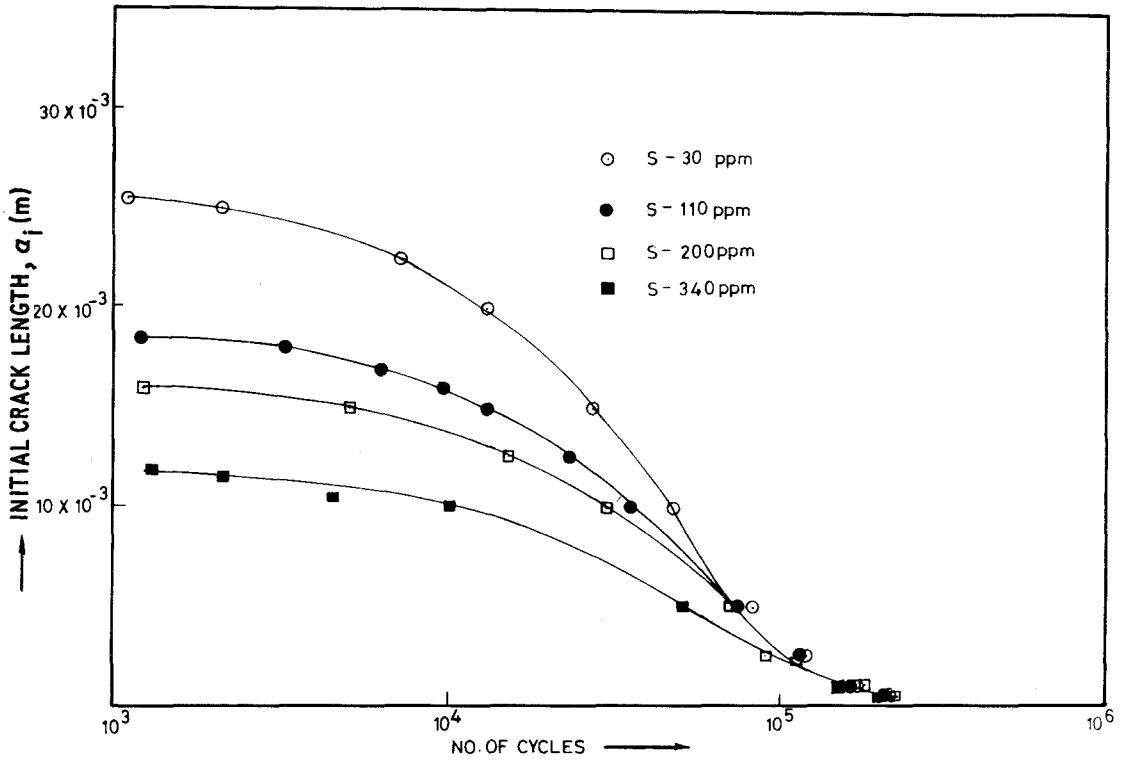

Figure 14 Relationship between crack length and number of cycles to failure for steels with different sulphur levels.

0.1 and different a values from the minimum detectable flaw size to the appropriate critical flaw sizes, the number of cycles required to cause failure has been calculated. The resulting curves are presented in Fig. 14. These curves represent the most convenient form of presenting fatigue data and enables the evaluation of the residual life after periodic inspections. It is evident that the maximum initial flaw size is longer for S–30 ppm steel compared with S–340 ppm. This offers additional justification for the use of electroslag refined or vacuum remelted steels, with lower sulphur levels than 110 ppm.

Similar results have been obtained by Logsdon [26] for AISI 430 modified 12Cr rotor steel based on high temperature fracture toughness and fatigue crack growth data. While the above curves are empirical, detailed stress analysis and experiments at appropriate temperatures need to be performed, so that from a knowledge of the defect geometry and various cyclic ranges of interest, the residual life of the component can be evaluated with certainty.

5. Conclusions

(a) Sulphide inclusions systematically and significantly affect the fracture toughness values in 12 wt% Cr steels.

(b) Inclusions with a size of 2 to 4 μm occurs with maximum frequency and the inter-sulphide inclusion spacing exhibits a more meaningful correlation with fracture toughness and the crack opening displacement than the percentage volume fraction.

(c) Sulphide inclusions do not significantly affect the fatigue crack growth rates. However, the sulphide inclusions affect the residual fatigue life in terms of tolerable crack length.

Acknowledgement

The authors wish to thank Dr A. Gopalakrishnan, General Manager and Dr R. Somasundaram, Laboratory Manager, Corporate R&D Division, Bharat Heavy Electricals Limited for their encouragement and permission to publish this paper. Thanks are due to Dr S. R. Valluri, Director, National Aeronautical Laboratory, for providing the laboratory facilities.

References

1. C. E. SIMS, *Trans. AIME* 215 (1959) 367.
2. A. J. BAKER, F. J. LAUTA and R. P. WEI, *ASTM*

STP number 370 (American Society for the Testing of Materials, Philadelphia, 1965) p. 3.
3. A. J. BIRKLE, R. P. WEI and G. E. PELLISSIER, *Trans. ASM* **59** (1966) 981.
4. J. M. KRAFFT, *Appl. Mater. Res.* **3** (1964) 88.
5. W. A. SPITZIG, *ASTM STP* number 453 (American Society for the Testing of Materials, Philadelphia, 1969) p. 90.
6. J. F. COPELAND, *J. Pressure Vessel Techn. (Trans. ASME)* 98 (1976) 135.
7. W. B. MORRISON, *Metals Tech.* **2** (1975) 33.
8. R. SCOTT, *ibid.* **2** (1976) 71.
9. S. K. CHAUDHARY and R. BROOK, *Int. J. Fract.* **12** (1978) 101.
10. P. PARIS and F. ERDOGAN, *J. Basic Eng. (Trans. ASME)* **85** (1963) 528.
11. D. BROEK, "A study on ductile fracture" NLR TR 71021 U (National Lucht en Ruimtevaar Laboratorium, The Netherlands).
12. M. H. JONES and W. F. BROWN, *ASTM SPT* number 463 (American Society for the Testing of Materials, Philadelphia, 1970) p. 63.
13. J. C. RITTER, *Eng. Fracture Mechanics* **9** (1977) 529.
14. J. R. RICE and M. A. JOHNSON in "Inelastic Behaviour of Solids", edited by Kanninen *et al.* (McGraw Hill Book Co., New York, 1971) p. 641.
15. D. BROEK, "Elementary Engineering Fracture Mechanics" (Sijthoff Noordoff, Netherlands, 1978) p. 279.
16. G. T. HAHN and A. R. ROSENFIELD, *Met. Trans.* **6A** (1973) 653.
17. J. M. BARSOM and S. T. ROLFE, *ASTM STP* number 466 (American Society for the Testing of Materials, Philadelphia, 1970) p. 281.
18. E. IRWING and L. N. McCARTNEY, *Met. Sci.* **11** (1977) 351.
19. K. NISHIOKA, K. HIRAKAWA and I. KITAURA, *Sumitomo Search* **17** (1977) 39.
20. A. M. SULLIVAN and T. W. KROOKER, *J. Pressure Vessel Technol. (Trans. ASME)* **98** (1976) 179.
21. A. OHATA and E. SASAKI, *Eng. Fract. Mech.* **9** (1977) 302.
22. G. R. IRWIN, *J. Appl. Mech.* **84E** (1962) 651.
23. ASTM Hand Book, *Mater. Res. Stand.* **4** (1964) 107.
24. H. D. GREENBERG, E. T. WESSEL, W. J. CLARK, Jr and W. H. PRYLE, Paper No. 69-109-MEMTL-p1. (Westinghouse Research Laboratories, Pittsburgh, 1969).
25. E. T. WESSEL, W. G. CLARK, Jr and W. K. WILSON, Report No. DDC-AD 801001 (Westinghouse Research Laboratories, Pittsburgh, 1966).
26. W. A. LOGSDON, *Eng. Fracture Mechanics* **7** (1975) 23.

Received 30 October
and accepted 15 December 1981